Structure and downstream evolution of the Agulhas Current system during a quasi-synoptic survey in February–March 2003

Tânia G. D. Casal,[1] Lisa M. Beal,[2] Rick Lumpkin,[3] and William E. Johns[2]

[1] The Agulhas Undercurrent Experiment took place in February–March 2003 off the east coast of South Africa and consisted of four sections of hydrographic and velocity data across the Agulhas Current between 30 and 36°S and connecting offshore sections that formed three closed boxes. An inverse model was applied to the quasi-synoptic data, and results show that the net mass transport at the historical 32°S section had a considerably higher transport of 100 ± 9 Sv than earlier estimates. This high transport falls within the peak-to-peak variability obtained previously from a current meter time series. Several mesoscale cyclonic eddies extending down to intermediate depths were sampled during the survey; in particular, a strong, locally formed shear edge eddy was found inshore of the Agulhas Current at 36°S. Offshore eddies were found to drive considerable onshore-offshore fluxes, resulting in highly variable Agulhas transports from one section to another. After attempting to account for and remove the influence of these eddies on the Agulhas transport, the downstream growth of the Agulhas Current is found to be consistent with the Sverdrup transport variation, within errors. To account for the total magnitude of the Agulhas transport, fluxes from both the Indonesian Throughflow and Indian Ocean overturning must also be taken into account. There is no clear evidence from this study for a significant contribution of inertial recirculation to the Agulhas within this latitude range.

1. Introduction

[2] Western boundary currents (WBC) of subtropical gyres close the interior circulation arising from net wind and thermohaline forcing and constitute the main pathways for communication between the equator and the polar regions [*Hogg and Johns*, 1995]. The average wind stress in the Southern Indian Ocean is predominantly eastward south of 32°S and reverses to the north [*Hellerman and Rosenstein*, 1983] driving a strong subtropical circulation of interior flow equatorward and a poleward WBC [*Toole and Warren*, 1993]. This WBC is the Agulhas Current; it flows southwestward along the steep continental slope of the east coast of South Africa between 27°S and 37°S carrying warm waters poleward. Once it extends beyond the tip of Africa, it retroflects toward the east feeding the Agulhas Return Current (ARC) that flows as a quasi-stationary meandering jet of troughs and ridges [*Boebel et al.*, 2003b] between 38°S and 40°S (Figure 1). As the Agulhas Current retroflects, it periodically sheds large eddies called Agulhas Rings [*Duncan*, 1968; *Gordon*, 1985; *Boebel et al.*,

2003a; *van Veldhoven*, 2005] that advect into the southern Atlantic Ocean and make a significant contribution to the heat and freshwater budgets of the Atlantic Ocean and thus play a role in the global thermohaline circulation [*Boebel et al.*, 2003a; *Lutjeharms*, 2006; *De Ruijter et al.*, 1999a; *van Veldhoven*, 2005]. The Agulhas Undercurrent, a potentially important route for ventilation of the deep Indian Ocean [*Beal and Bryden*, 1997] flows as a countercurrent beneath the Agulhas Current.

[3] Typical subtropical western boundary currents, such as the Agulhas Current, are characterized by a width of 50 to 150 km, strong lateral velocity gradients, a central warm core with speeds higher than 1 m s^{-1} [*Pearce*, 1977; *Pearce and Gründlingh*, 1982] and a density structure with isopycnals sloping sharply upward toward the coast.

[4] The full depth direct velocity field of the Agulhas Current has been measured in several experiments using a lowered acoustic Doppler current profiler (LADCP). In February–March 1995, at 32°S off the east coast of South Africa, the Agulhas Current exhibited speeds exceeding 180 cm s^{-1} at its core 20 km offshore [*Beal and Bryden*, 1999]. The current was 90 km wide between the 50 cm s^{-1} isotachs and its maximum offshore extent was 200 km. The Agulhas Undercurrent, a persistent feature with peak velocities of 30 cm s^{-1} and an annual mean velocity of 10 cm s^{-1} northward [*Bryden et al.*, 2005], flowed beneath the Agulhas

[1]CIMAS, RSMAS, University of Miami, Miami, Florida, USA.
[2]MPO, RSMAS, University of Miami, Miami, Florida, USA.
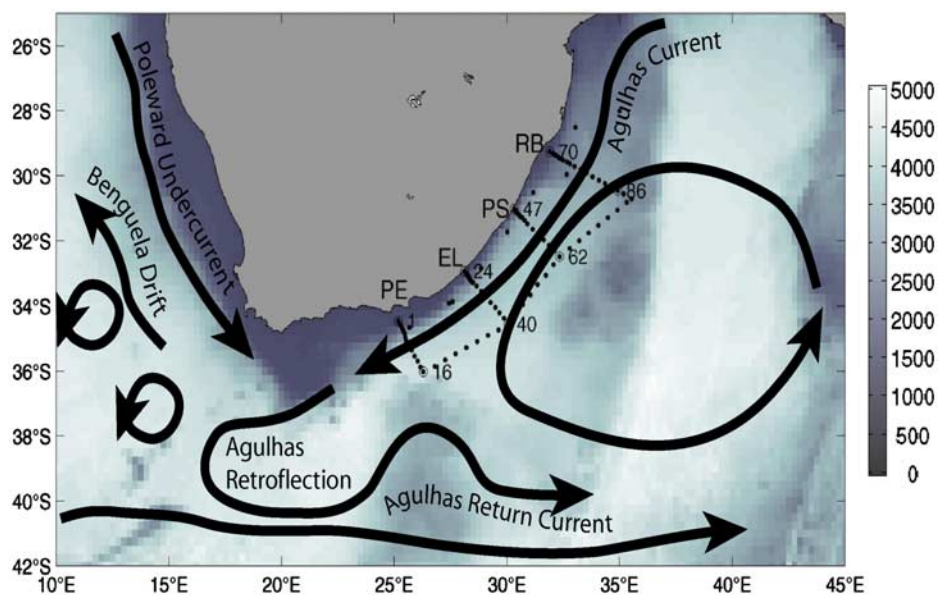[3]PhOD, AOML, NOAA, Miami, Florida, USA.

Figure 1. Schematic of the traditional view of oceanic flow patterns around southern Africa. Stations occupied during AUCE are overlaid, and the beginning and end stations of each section are numbered. PE refers to Port Elizabeth (36°S) sampled from 20 to 23 February 2003. EL refers to East London (34°S) sampled from 25 to 27 February, PS refers to Port Shepstone (32°S) sampled from 1 to 3 March, and RB refers to Richards Bay (30°S) sampled from 5 to 7 March 2003. Color bar is the bottom topography in meters.

Current in the opposite direction (northward) at approximately 1200 m [*Beal and Bryden*, 1997].

[5] *Beal and Bryden* [1999] showed that the Agulhas Current at 32°S was in geostrophic balance below 200 m, with a full water column transport of 73 Sv referenced to LADCP versus a 75 Sv transport from LADCP velocities alone. As for the Agulhas Undercurrent, the transport was 5 Sv. *Donohue et al.* [2000] found a similar structure along the same transect during March and June 1995 and estimated the net transport to be 78 and 76 Sv respectively, with an Agulhas Undercurrent transport of 3.6 and 5.4 Sv respectively.

[6] Recently, *Bryden et al.* [2005], using yearlong mooring data, computed the total transport for the 267 days of best instrument coverage of the Agulhas Current as 69.7 Sv with a standard deviation of 21.5 Sv, calculated from the surface to 2400 m depth and from the coast to 203 km offshore. The Agulhas Undercurrent was measured with an average equatorward transport of 4.2 Sv.

[7] These transports are smaller than those previously obtained by *Toole and Warren* [1993], who estimated a geostrophic transport of 85 Sv for the same section using data from November–December 1987. The difference in transport was attributed to the use of different reference levels. *Bryden and Beal* [2001] applied a zero velocity surface (ZVS) approximated by their LADCP measurements to *Toole and Warren*'s [1993] section and obtained a considerably smaller transport of 63.3 Sv. All these transports are roughly consistent with historic work by *Gründlingh* [1980], who estimated an Agulhas Current baroclinic volume flux of about 62 Sv in the upper 1000 m for five repeat sections near 30°S.

[8] Overall, the congruence of the transports from LADCP sections, hydrographic sections referenced to LADCP, and current meters suggest an average Agulhas Current transport of about 70 ± 8 Sv near 30°S to 32°S [*Bryden and Beal*, 2001; *Bryden et al.*, 2005], which makes it the strongest of all western boundary currents (including the Gulf Stream) when measured at similar latitudes [*Bryden et al.*, 2005]. *Bryden et al.* [2005] noted that the Agulhas Current transport was considerably larger, by about 25 Sv, than the Sverdrup transport implied from the wind stress curl over the interior Indian Ocean.

[9] One component of the WBC transport not taken into account by the Sverdrup relation is inertial or eddy-driven recirculations. In the detached Gulf Stream, these recirculations, located both to the north and south of the Gulf Stream, have been shown to be nearly barotropic in nature [*Cessi et al.*, 1987; *Hogg*, 1992; *Johns et al.*, 1995] and to greatly increase the downstream transport. *Feron et al.* [1998] have shown that such inertial recirculations must exist at the separations of all major boundary currents.

[10] In this paper, we use in situ measurements to construct a mass-conserving description of the Agulhas Current system during February–March 2003. In particular, we investigate the eddy field along the Agulhas Current and its downstream evolution, including velocity structure and transport changes. Our analysis is augmented by the use of satellite and wind data over the period of the measurements. Finally, we consider how its evolution corresponds to wind forcing, thermohaline forcing, and local inertial recirculations, whose relative roles have not previously been quantified for the Agulhas Current.

2. Data

2.1. AUCE Hydrographic Data

[11] The Agulhas Undercurrent Experiment (AUCE) took place aboard R/V *Melville* between 14 February and

17 March 2003 off the east coast of South Africa (Figure 1). The field experiment consisted of four cross-stream sections of the Agulhas Current system, nominally at 30°, 32°, 34°, and 36°S, plus three along-stream sections offshore of the Current and about 250 km from the coast. The cross sections were on average 200 km long and took 3 days to sample and the offshore sections were about 350 km long and were sampled in a day (wider station sampling). Together, these sections divided the western boundary region into three closed boxes (Figure 1). Observations have shown that solitary meanders [Lutjeharms and Roberts, 1988; De Ruijter et al., 1999b; van Leeuwen et al., 2000] are the dominant form of variability in the Agulhas Current along the African coast [Bryden et al., 2005] and are related to offshore anticyclones [Schouten et al., 2002]. Four to six of these meanders typically occur over the course of a year, for this reason, prior to each cross section of the Agulhas Current, an underway shipboard ADCP (SADCP) section was occupied to identify the position and width of the jet in case it had meandered offshore, allowing the station positions to be adjusted according to the instantaneous structure and position of the current. The SADCP was an RD Instruments 150 kHz narrowband instrument which profiled consistently to depths of about 200 m and up to 300 m. Final ocean velocities have an estimated accuracy of 1–2 cm s^{-1}. Station spacing for the cross-stream sections was as little as 5 to 10 km over the shelf break and continental slope in order to resolve the strong cyclonic shears in the current there. Spacing increased to no more than 30 km farther offshore. Along the offshore sections, station spacing of 50 km was used owing to expected longer correlation length scales along the direction of flow. Each station consisted of full-depth casts of a combined CTDO$_2$/LADCP package with 24 bottles for salinity and oxygen calibration, plus an altimeter to find range off the bottom. LADCP data were collected with an RD Instruments 150 kHz broadband instrument with 30 degree beam angles and converted to absolute velocities using a least squares inversion (A. Thurnherr, RDI LADCP Cruise Report, Aurora Australis Voyage 4, 2003, unpublished report, 2003, available at ftp://ftp.ldeo.columbia.edu/pub/ant/LADCP/A0304/LADCP_CruiseReport.pdf). The inversion constrained the calculated shear solution following the approach of Firing [1998] and Fischer and Visbeck [1993], to position data, near-surface SADCP velocities, and bottom-track velocities. The bottom-track velocities were extracted using a combination of water track and beam amplitude data [Visbeck, 2002]. Errors were estimated a posteriori from the inversion as a maximum 2 cm s^{-1} in the deep water and above the bottom-tracking region (below 1500 m and above 100 m from the bottom) and a minimum 0.5 cm s^{-1} within the depth of the SADCP data (250 m from the surface). However, these errors do not include measurement noise, which we estimate later.

2.2. Altimetry

[12] We use AVISO altimeter products, which were produced by the CLS Space Oceanography Division as part of the Environment and Climate EU ENACT project (EVK2-CT2001-00117) and with support from CNES. AVISO sea level anomalies are derived from merged TOPEX/Poseidon and ERS-1 data [Le Traon and Ogor, 1998]. To find absolute sea level, we superimposed these anomalies on the Rio05 mean dynamic topography [Rio and Hernandez, 2004], which was derived from a combination of GRACE gravity measurements, Levitus and Boyer [1994] climatology, altimetry, and drifter trajectories.

[13] In addition, we use an altimeter proxy time series of geostrophic Agulhas Current transport over the upper 1000 m produced by Gustavo Goni (NOAA) and available at http://www.aoml.noaa.gov/phod/altimetry/cvar/agu/transport.php. This time series was derived from 10-day AVISO sea surface height anomaly fields from satellite altimetry, together with Levitus and Boyer [1994] climatological mean dynamic topography relative to 1000 m.

2.3. Wind

[14] Monthly values of the wind stress curl spanning August 1999 to January 2006 were obtained from CERSAT (IFREMER) at http://www.ifremer.fr/cersat/en/data/download/gridded/mwfqscat.htm. This product provides synoptic gridded fields (0.5° × 0.5° resolution) of wind parameters obtained from the NASA SeaWinds scatterometer on board QuikSCAT. The discrete observations over each time period are statistically interpolated using an objective method to reconstruct gap-filled and averaged synoptic fields.

3. Box Inverse Model Methodology

[15] The data collected during AUCE represent a quasi-synoptic survey of a highly variable current system. During our monthlong survey, fluctuations associated with the appearance and advection of mesoscale features and meanders, and with barotropic waves and tides were all aliased in our measurements. Nevertheless, an inverse model approach was considered beneficial in order to build the most consistent picture of the transports during AUCE, by balancing known conservative quantities. In addition, by conserving mass, we could minimize measurement errors from instrument noise and temporal variability. The disadvantage of an inverse model approach is that a nonsynoptic data set is constrained as if it were synoptic. However, we argue that traditional treatments of nonsynoptic survey data implicitly make such an assumption, but without formalizing errors as we can by executing an inversion.

[16] The inverse model [Lumpkin and Speer, 2003] solves the conservation equations for mass, salt anomaly (with respect to 35 psu) and heat anomaly (with respect to 0°C) inferring isopycnal and diapycnal transports from property budgets within isopycnal oceanic layers. The unknowns of the system of equations are the reference velocities for each station pair and the diapycnal fluxes for density, heat and salt across each interface within each box. Because we had more unknowns than equations, this system was underdetermined with an infinite number of solutions requiring a least squares technique, the Gauss-Markov estimation [Wunsch, 1996], to find the "best" solution. For more details on the methodology, the reader is referred to Lumpkin and Speer [2003].

[17] Geostrophic velocities between each station pair were only determined to the deepest common level (DCL) of the stations and therefore, estimation of the property transports in the bottom triangles below the DCL was required. This was particularly important for the Agulhas Current where topography is steep. Throughout this study,

the "constant velocity" method is used to determine the transport in the bottom triangles [*Ganachaud*, 1999], where it is assumed that the velocity at the DCL, between two stations is constant below the DCL. The errors introduced with this particular method versus constant shear, for example, were relatively small, 0.2 Sv in the lower deep layer where the net transport error bars was of ~3 Sv.

[18] In outcropping layers, strong diapycnal transfers can be driven by lateral eddy fluxes, mixed layer entrainment, and air-sea exchanges. Therefore, in these layers, mass, heat and salt are not conserved. We defined outcropping layers by calculating the mixed layer depth (MLD) as the depth in which the temperature differed from that at 6 db by $1.0°C$, following *Chereskin and Roemmich* [1991]. We found that the MLD varied from 5 m over the continental slope to a maximum of 105 m offshore. Hence, we relaxed conservation constraints in all layers that outcropped to 105 m, that is, within layers 1 to 7, corresponding to a neutral density value of 26.15.

[19] Prior values of air-sea heat and freshwater fluxes were set to zero because the small area of the AUCE boxes yielded negligible air-sea fluxes compared to the allowed error in heat conservation of O(~0.1 PW) (e.g., multiplying an absolute net heat flux for March of 100 W m^{-2} by the area of the largest box yielded a value of 0.01 PW, considerably smaller than the error estimate of a heat transport estimate). Since the three processes that affect diapycnal fluxes in the mixed layer are heat and freshwater exchanges with the atmosphere (set to zero in our case), mixed layer entrainment and lateral eddy fluxes, we assumed diapycnal fluxes were dominated by the latter two processes, in particular lateral eddy fluxes. Such an assumption seemed reasonable given the high eddy kinetic energies associated with western boundary currents. Ekman fluxes were also negligible (between 0.05 to 0.11 Sv) compared to error tolerances in the surface layers of 1 Sv, and as a consequence, the Ekman fluxes were also neglected.

[20] Isopycnal flux estimates were obtained from the inverse model applied to the geostrophic velocity shears. The inverse model also solved for the diapycnal fluxes, which resulted from all mixing processes that act to transfer mass, heat and salt between water masses. These fluxes included advection, diffusion, and eddy fluxes. Following *Sloyan and Rintoul* [2000, 2001] we used independent interior mixing flux unknowns for each property (w_m^*, w_h^* and w_s^*). The interior diapycnal mixing of density, salt and heat were all given a prior (preinversion) value of zero. The allowed variance of the mixing terms for mass, heat and salt was given by the prior convergence or divergence of the property of the layer [cf. *Lumpkin and Speer*, 2003]. Since the outcropping layers were given much larger errors, the diapycnal fluxes in these layers (which could be horizontal and large) had much larger errors compared to the deeper diapycnal fluxes which are in general small and vertical [*Lumpkin and Speer*, 2003].

[21] To take into account asynoptic effects during the survey, each section was assigned a net error T$_{ap}$ to account for noise from time variability. Mass over each box was conserved to within ±5 Sv for full depth and ±0.2 Sv for individual layers below the MLD. This resulted in a section error, or $T_{ap} = \sqrt{\frac{(box\ error)^2}{3}} = 2.9$ Sv. The model error in heat

conservation was given by the layer's volume error multiplied by the sum of the mean potential temperature in each layer (θ), and twice the standard deviation of θ within the layer, in each hydrographic section bounding the box. A similar procedure was used for the salt conservation, using a salinity anomaly given by (S − 35)/1000 [*Ganachaud*, 2003].

[22] Finally, it must be stressed again that even with the use of an inverse model, our measurements during AUCE cannot be considered representative of the mean state of the system. Rather, the data obtained during AUCE provide a quasi-synoptic description of the Agulhas that can be viewed as, at best, a seasonal snapshot of the system. Nevertheless, using an inverse model, the estimated transports and diapycnal fluxes can be determined consistently and with assigned error bars.

3.1. Experimental Setup

[23] We conducted two inverse experiments, the first one using only the CTD data (geostrophic experiment) and the second one incorporating LADCP data for the level of no motion (LADCP experiment), representing two reasonable initial states. For the geostrophic experiment, the level of no motion (LNM) was given by a neutral surface separating water masses which are expected to flow in opposite directions [*Toole and Warren*, 1993]. In our particular case, the LNM was given by the neutral surface that separated the southward flowing intermediate layer and northward flowing upper deep layer (corresponding to $\gamma = 27.92$). The estimated uncertainty of these reference velocities, which sets the allowed range of the inversion, was chosen as ±10 cm s^{-1}. The choice of error arose from examination of the LADCP velocities where values of 10 cm s^{-1} were found intercepting the neutral surface set up as the LNM. Errors of 10 cm s^{-1} are a typical WBC adjustment in models such as *Ganachaud et al.* [2000] and *Lumpkin and Speer* [2003]. It should be noted that this type of inversion is usually the first step in approaching such a problem and represents the only available way of setting up an inverse model in the absence of any direct velocity data.

[24] In the LADCP experiment, direct velocity information was used to estimate an initial reference velocity. A simple way to incorporate the LADCP observations would have been to extract absolute velocities at the geostrophic reference level and add them to the thermal wind profiles. However, this can be inaccurate because of the small-scale, ageostrophic structures present in the LADCP data. To mitigate this effect, we set the reference velocity as the mean of the difference between the LADCP and geostrophic profiles. Furthermore, because the upper water column was dominated by ageostrophic wind-driven effects, the mean of the difference between the LADCP and geostrophic profiles was calculated below 100 m. The error for this reference velocity was decided upon two criteria: analysis of the spatial variability of the LADCP solution error (given by the LADCP inversion, as described in section 2) and any additional sources of error such as measurement error, internal waves and wind-driven barotropic motions. Hence, we estimated an error of ±5 cm s^{-1}. Our objective was to assess how dependent the box model is on initial conditions (LNM or LADCP) and evaluate if there were any improvements in the results by including the LADCP information.

Table 1. Inverse Model Layers, Neutral Surface Densities, and Upper Bound Limit on the Layer Error

Layers	Layer Number	Neutral Surface Densities	Upper Bound Error (cm s^{-1})
Surface	1–6	$21.4 \leq \gamma \leq 25.0$	relaxed, 500
Subsurface	7–8	$25.60 \leq \gamma \leq 26.15$	relaxed, 500
Thermocline	9–10	$26.560 \leq \gamma \leq 26.855$	constrained, 5
Intermediate	11–21	$27.070 \leq \gamma \leq 27.895$	constrained, 5
Upper deep	22–32	$27.925 \leq \gamma \leq 28.075$	constrained, 5
Lower deep	33–45	$28.085 \leq \gamma \leq 28.400$	constrained, 5

3.2. Inverse Model Solutions

[25] Before discussing our scientific results, we first examine the differences between the circulations from our two inversions, namely the geostrophic and LADCP experiments, to determine which solution has more skill.

[26] The inverse model run for the geostrophic experiment revealed that the property conservation equations were well resolved, i.e., conservation of mass, heat and salt provided independent information in all three boxes with the exception of the northern most box, where mass was only weakly resolved. In the LADCP inverse model run, on the other hand, mass and heat were well resolved in all 3 boxes whereas salt was weakly resolved in the northern most box. In both experiments, inverse model reference velocities were within the a priori range.

[27] To more clearly illustrate our inverse model solutions for the Agulhas Current system, six blocks of layers were defined (Table 1) separating the water column into the surface layer (given by the sum of the top 6 layers), the subsurface layer (the sum of layers 7 and 8), the thermocline layer (the sum of layers 9 and 10), the intermediate layer (the sum of layers 11 to 21), the upper deep layer (the sum of 22 to 32) and finally the lower deep layer (sum of the bottom 13 layers). These layers correspond to the main water masses present: tropical surface water, subtropical surface water, thermocline waters, Antarctic intermediate water and Red Sea water, and finally upper and lower North Atlantic deep water.

[28] The mass fluxes resulting from the LADCP experiment are shown in the schematic of Figure 2. Error bars were much smaller in the LADCP experiment compared to the geostrophic experiment (not shown), a direct consequence of the smaller allowed adjustments. This in turn, led to estimates that were significantly different from zero for the deep layer isopycnal transports and diapycnal fluxes. The major changes in the flow structure between the LADCP and geostrophic experiment occurred in the intermediate and deep layers, with the surface and thermocline layers yielding comparable transports. Other differences found were the inflow/outflow from the offshore sections, particularly the one connecting Port Shepstone (32°S) and Richards Bay (30°S), which increased significantly (∼30 Sv) in the LADCP experiment versus the geostrophic one. At first, we suspected that the offshore increase was introduced in the inverse model solution to conserve the properties within the specified 5 Sv, but a close look at the a priori mass transport values and LADCP profiles versus geostrophic profiles (not shown) revealed that in fact a considerable flow through the offshore sections exists with significantly nonzero velocities at the LNM of the geo-

strophic calculation. The latter was substantiated by altimetry data (Figure 3), showing that these flows were associated with intense cyclonic and anticyclonic circulations (with speeds of the order of 25 cm s^{-1} and higher). These features will be considered in more detail later.

[29] In the upper layer of deep water between $27.92 < \gamma < 28.08$, the LADCP experiment, when separated into individual station transports, clearly showed an undercurrent against the African continental slope (Figure 4). The Agulhas Undercurrent transport in this layer ranged from 4.2 ± 0.9 Sv at the Port Elizabeth section (36°S) to 2.8 ± 2.1 Sv exiting at Richards Bay (30°S), where it was offshore of the Agulhas Current core because of the shoaling topography. These results suggest that the Undercurrent represents a continuous northward flow of upper North Atlantic Deep Water (NADW), in agreement with *Van Aken et al.* [2004] and *Arhan et al.* [2003], who found evidence for a NADW slope current rounding South Africa from the South East Atlantic and flowing into the Mozambique Channel. Their estimates were for 2–3 Sv of transport. No such undercurrent was found in the geostrophic experiment because of the water mass based LNM (not shown).

[30] The largest discrepancy between the experiments lied in the diapycnal transports. Each experiment revealed generally different values (some of them comparable to the maximum allowed mass imbalance within each box) and direction and no consistent pattern was revealed, therefore we did not regard them as robust and will not attempt to interpret these diapycnal transports.

[31] On the basis of the points discussed above, we decided to choose the LADCP experiment as the solution with the most skill with regards to the horizontal mass transports. In the following section we use this solution to describe the Agulhas Current system during AUCE.

4. Results

4.1. Transport at the Historic 32°S Section

[32] The section-integrated mass transport at Port Shepstone (Figures 2 and 5) was 100.3 ± 9.4 Sv flowing southward. This is considerably higher than the mean of 69.7 ± 21.5 Sv obtained by *Bryden et al.* [2005] from a nearly yearlong current meter time series and the 76 Sv from *Donohue et al.* [2000] for the 1995–96 mean of three sections. Nevertheless, *Bryden et al.* [2005] showed that the Agulhas Current daily transport at this location could be as high as 121 Sv or as low as 9 Sv, and thus it appears that we sampled the Agulhas Current at a time of near-maximum flow. A comparison with *Bryden et al.*'s [2005] Agulhas Current structure when the transport was largest (Figure 11b of *Bryden et al.* [2005] versus our Figure 6b) revealed a similar velocity pattern to ours, with the depth of the 50 cm s^{-1} isotach around 900 m in both realizations. *Bryden et al.* [2005] assumed zero velocity at 2400 m depth and this could also explain some of the difference in transport, since the AUCE section has a significant barotropic component. This strong barotropic flow at Port Shepstone (32°S, Figure 6b) appeared to be associated with barotropic eddies and waves, since it is not seen in other sections. We will discuss these ideas further in section 4.3 below. The barotropic tide in the Agulhas Current region is of O(1
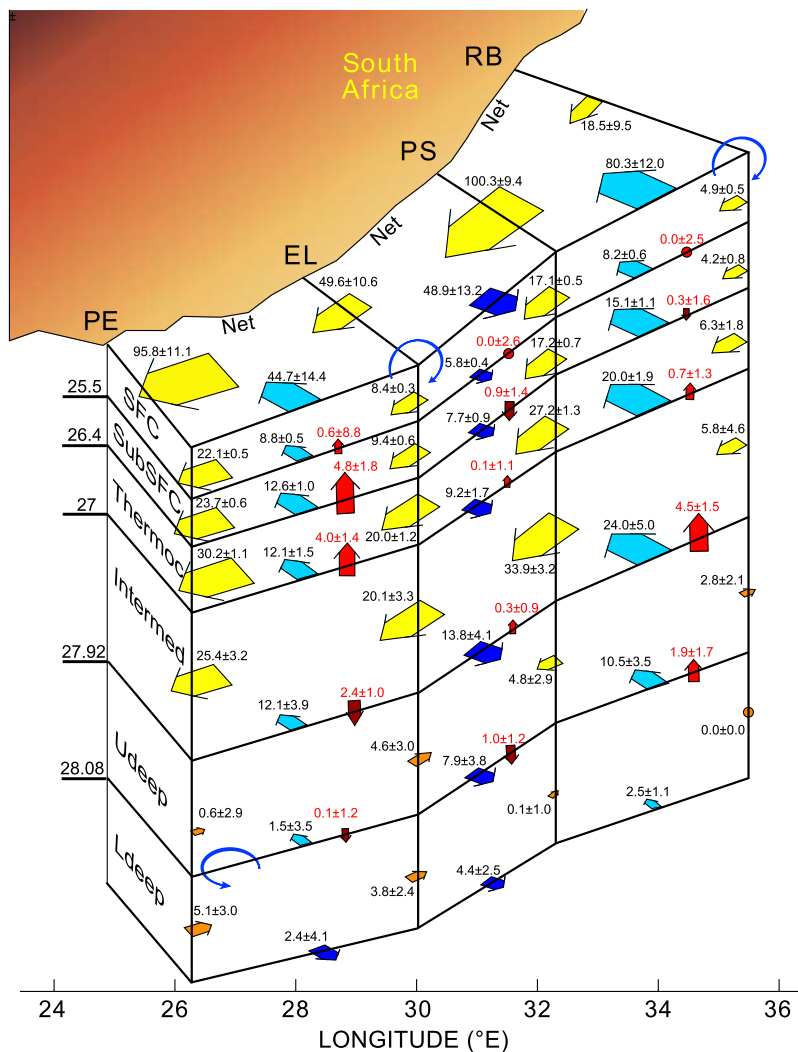
Figure 2. Inverse model mass transport (in Sv) and standard errors for the Agulhas Current system for the LADCP experiment. Net mass transport values are displayed on the top, and each individual layer displays the mass transport associated with it. Red arrows represent diapycnal transports, and blue, yellow, and orange arrows represent isopycnal transports. Small circular arrows indicate the location of some of the sampled eddies.

cm s^{-1}) and certainly too small to have any influence in this pattern.

[33] Additional evidence for a strong Agulhas Current transport during AUCE comes from a NOAA proxy time series of geostrophic transport (assuming a LNM at 1000 m) of the Agulhas Current (Figure 7) clearly showing that 2003, in particular in the beginning of the year, exhibited higher geostrophic transports than 1995, even though the annually averaged values for the 2 years do not differ greatly. Comparison with the altimetry long-term mean suggests that during AUCE the transport was 8% higher than the mean, whereas in 1995, coinciding with *Bryden et al.* [2005] data set, it was 3% lower than the long-term mean. As validation of the altimeter proxy transports, we have superimposed our observed estimate for the upper 1000 m at East London during AUCE (Figure 7). This was the section closest to the altimeter proxy and the difference from the 2003 annual mean altimeter-inferred transport was less than 5 Sv.

[34] In order to proceed with an analysis of the downstream evolution of the Agulhas Current transport, it was first necessary to describe the eddies sampled during the experiment, since their influence needs to be accounted for when considering how to define the Agulhas Current and its related inflow/outflow fluxes.

4.2. Eddy Features and Their Influence on the Agulhas Current

[35] Our hydrographic data, together with the altimetry fields (Figures 3 and 6) showed that the Agulhas Current region is populated with a series of mesoscale eddies during the AUCE. Figure 5 is our schematic of fluxes in the region together with the position of the main eddy features. These features impact the width, depth, and position of the Agulhas Current as well as its transport, as it flows through the region. In particular, three cyclonic eddies were found in the AUCE in situ sections, one inshore of the Agulhas Current and the remaining two offshore (Figure 3). Anticy-
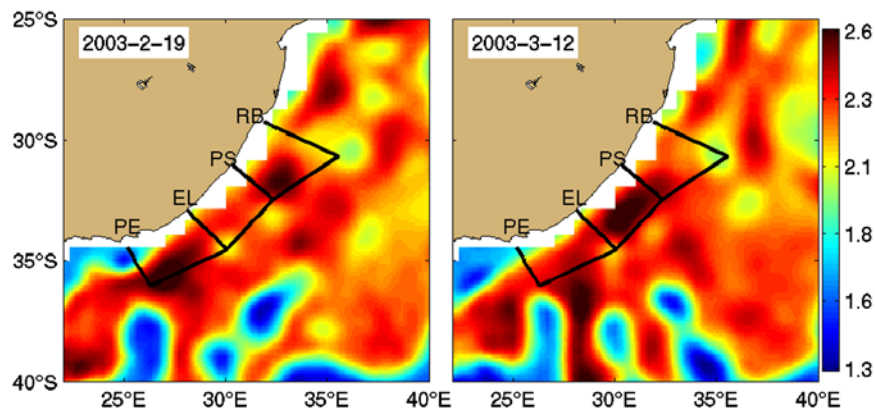
Figure 3. Absolute sea level during the AUCE survey (in m) with the AUCE cruise track overlaid. (left) Surface circulation on the day previous to the start of the Port Elizabeth sampling (PE). (right) Start day of the sampling of Richards Bay (RB).

clonic features are also observed, but are highly elongated, reminiscent of the offshore ridge of a Munk boundary layer [*Munk*, 1950; *Webb*, 1999]. In the analysis that follows (section 4) we attempt to remove the influence of all these features in the transport estimates for the Agulhas.

[36] Here we describe the three cyclones in detail. The largest cyclone was named the Richards Bay (RB) eddy (Figure 5) as it was sampled at the offshore end of this northernmost section. Specifically, it was sampled between stations 84 and 88 of the Richards Bay section (shown in vertical cross section in Figure 6a) and also seen in the offshore section (not shown) connecting Port Shepstone

(32°S) to Richards Bay (30°S). The RB eddy carried 21 ± 3 Sv of water and had a radius of 130 km. Eddy transports were defined as the integrated transport from the center of the eddy to the 5 cm s^{-1} isotachs (corresponding to the assigned error bar) and these values may be underestimated if the sections did not cut through the exact center of the eddy. The RB eddy's velocity structure extended to at least 1500 m, reaching into the intermediate layer. Its tangential speed was up to 50 cm s^{-1}, with maximum velocities found at 250 m depth, in the thermocline layer. Transports were significantly different between the RB eddy sampled in the offshore section and the same eddy sampled in the Richards
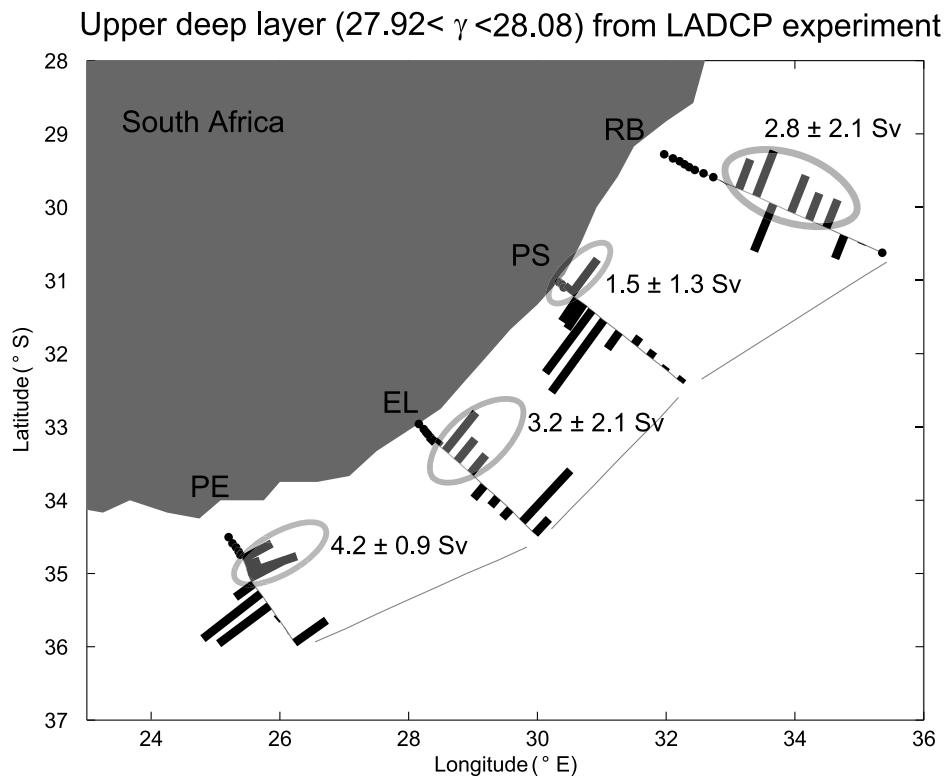

Figure 4. Mass transports for the Agulhas undercurrent and associated standard errors in the upper deep layer, in the LADCP experiment.
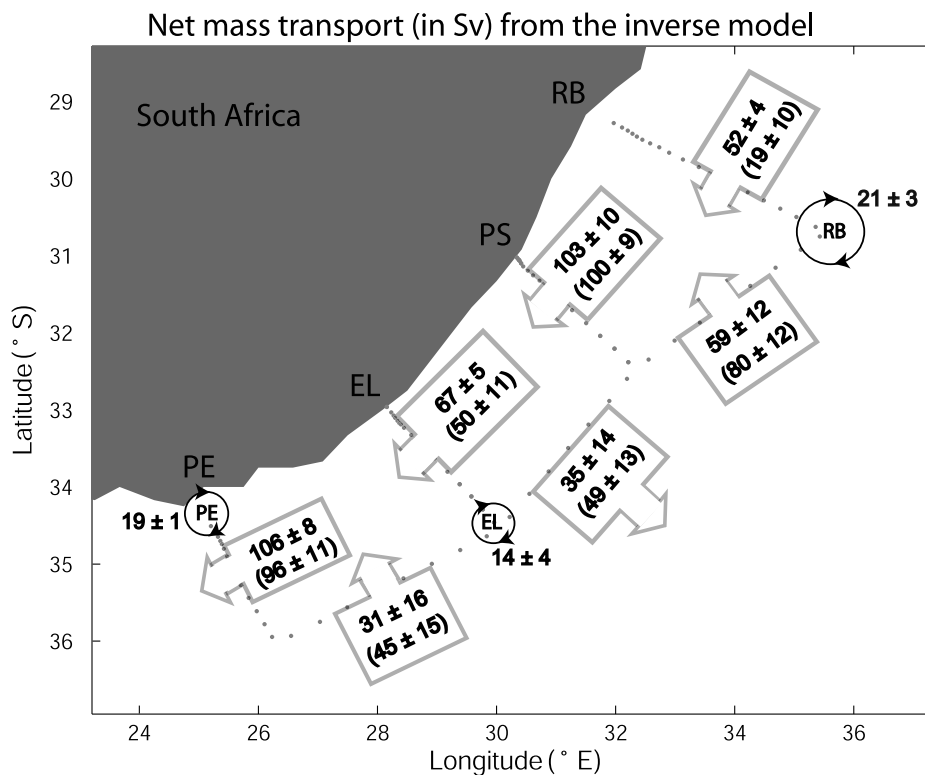
Figure 5. Inverse model net mass transport for the Agulhas Current system (in Sv). Alongshore values in parentheses are total cross-section transport versus the transport of the Agulhas Current only (as defined in the text). For the offshore sections, the values in parentheses indicate the total transport compared to the transport excluding eddy recirculation. The three sampled eddies and their respective transports are also shown.

Bay section, with the former more than double the outgoing transport at the latter. We interpret this as evidence that some of the eddy flow through the offshore section became entrained in the Agulhas Current, although it may have also resulted from temporal sampling aliasing, if the eddy translated southward between the occupations of the offshore line and the end of Richards Bay, for example. Analysis of the water properties within the eddy did not reveal any anomalous properties relative to its surroundings, which implies that this cyclone was a locally formed feature.

[37] Another cyclone, the East London (EL) eddy, was located at the offshore end of the East London section (Figure 5). It was smaller in size and transport than the RB eddy, with a 93 km radius and a transport of 14 ± 4 Sv, and also appeared to have been formed locally (Figure 6c, stations 36 to 40). The velocity structure of the EL eddy reached 1200 m depth, and had maximum tangential speed of 40 cm s^{-1} at the surface. Both RB and EL eddies influenced the inflow/outflow through the offshore sections since they accounted for about 30% of the total transport through those sections.

[38] The Port Elizabeth section (Figures 5 and 6d) at 36°S also revealed the presence of a cyclonic eddy, here enclosed between the landward side of the Agulhas Current and the shelf edge at stations 1 to 6 (Figure 6d). This eddy was the deepest and narrowest cyclone sampled, with a velocity structure extending to depths of 2000 m (the bottom of the

intermediate layer) with a radius of about 40 km and swirl transport of 19 ± 1 Sv. Analysis of consecutive altimetry images from before and after our occupation, suggest that this feature was a locally formed shear edge eddy [*Lutjeharms et al.*, 2003], which dissipated after a month at its site of formation, with no downstream propagation. The flow field here was reminiscent of that observed in the time series data of *Bryden et al.* [2005] at 31°S during a meander event (Natal Pulse). The Agulhas Current weakened and moved offshore and northward flow appears to penetrate upward from the undercurrent, eventually surfacing to exhibit a strong barotropic northward flow inshore of the Agulhas Current. Here, the Agulhas Current was farther offshore as a result of boundary separation rather than a meander, and the shear edge eddy has formed inshore. Strong barotropic northward flow was found, with potential temperature (not shown) and neutral density surfaces (in green in Figure 6) steeply rising over the continental slope. A second velocity core remained at depth, indicative of the presence of the Agulhas Undercurrent underneath the shear edge eddy.

4.3. Agulhas Current Transport and Growth

[39] To study the downstream evolution of the Agulhas Current transport, we carefully defined its boundaries to exclude eddies and counterflows described in the previous section. This is important because the sampled sections not only spanned the continuous WBC flow, but also included convergent and divergent fluxes from other features present
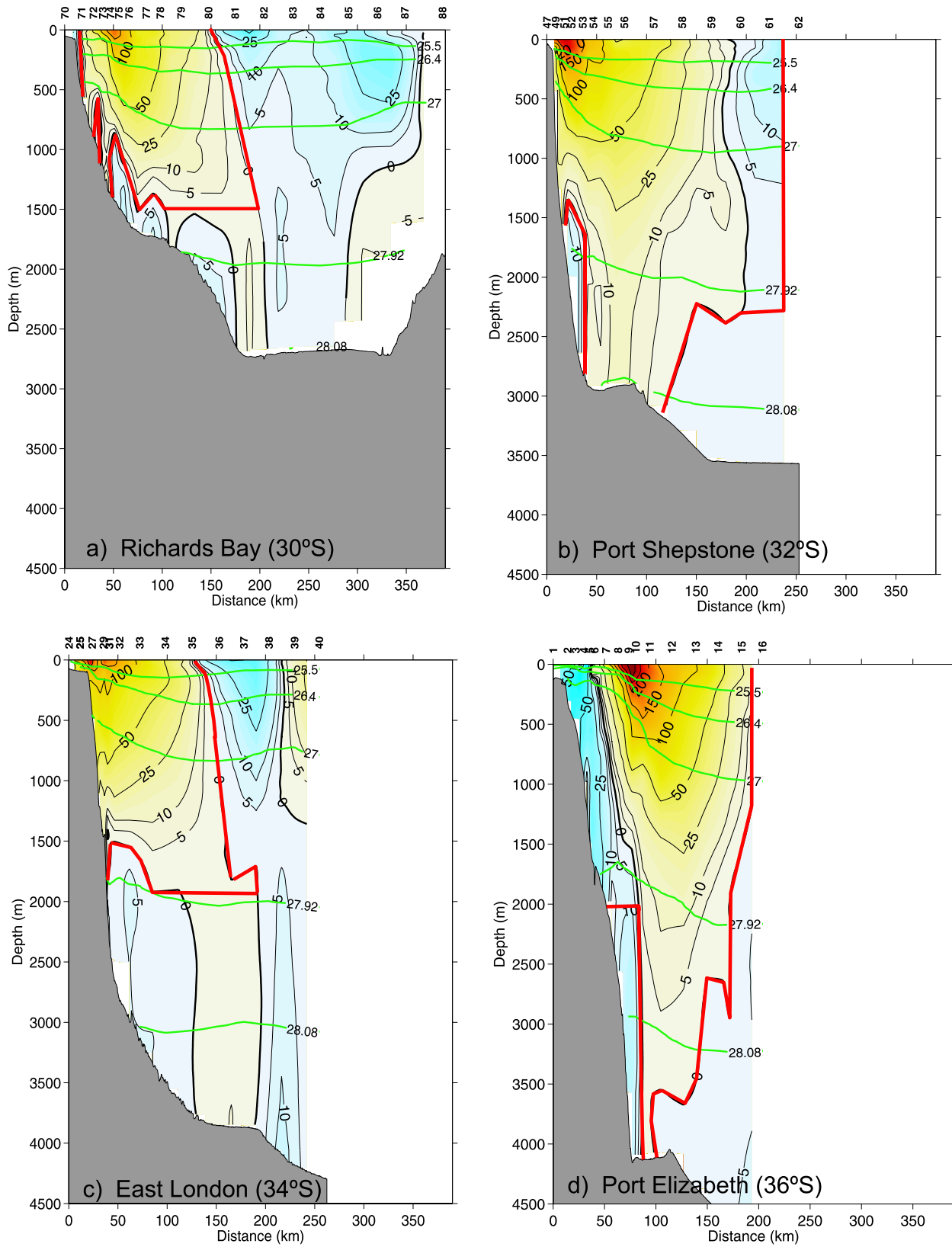
Figure 6. Inverse model derived velocities (in cm s^{-1}) in each cross section as a function of depth. The thick red lines delineate the Agulhas Current. Positive velocities (blue) indicate northward direction, and negative velocities (yellow) indicate southward direction. Heavy black line is the zero contour line. Station numbers are indicated on the top.
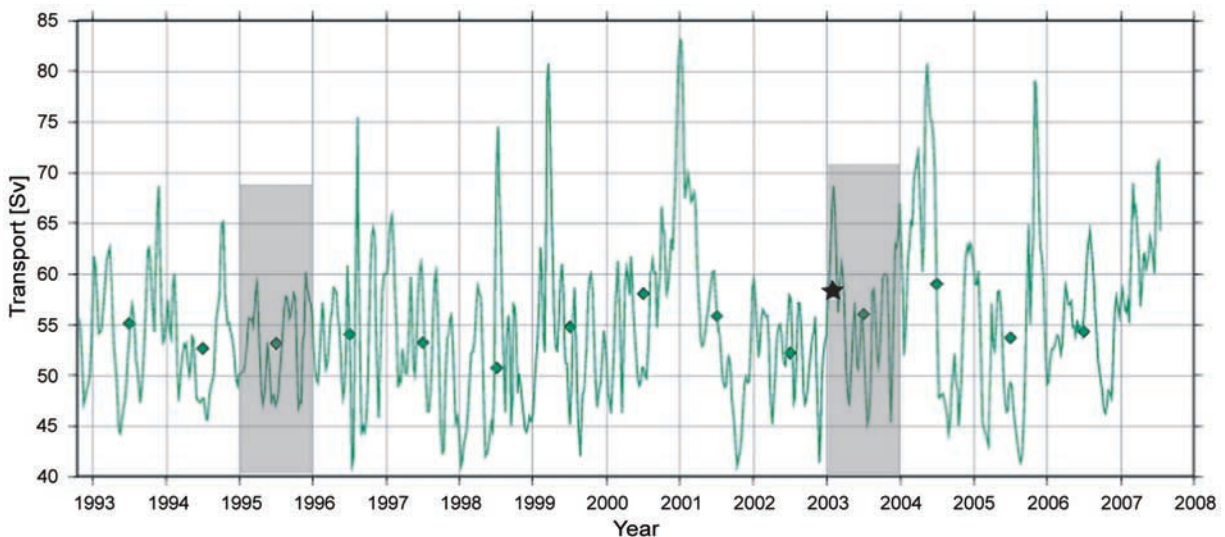
Figure 7. Time series of geostrophic transport of the Agulhas Current in the upper 1000 m assuming a LNM at 1000 m and using a combination of SHA, satellite altimetry (AVISO), and *Levitus and Boyer* [1994] climatological data at nominally 34°S (G. Goni and P. DiNezio, personal communication, 2006). Annual mean values are given by the diamonds (from http://www.aoml.noaa.gov/phod/altimetry/cvar/ agu/transport.php). Shaded rectangles highlight 1995 (the period studied by *Bryden et al.* [2005]) and 2003 (AUCE). For comparison, the inverse Agulhas Current transport for East London (34°S) in the upper 1000 m (58.9 ± 2.5 Sv) is represented by the star.

during the hydrographic observation period. The overall criteria selected to define the Agulhas Current boundaries were (1) only southwestward flow was considered if eddies were not sampled, with the boundary of the transport integration set as the 0 cm s^{-1} isotach (i.e., undercurrent and other northward flows excluded), and (2) contributions associated with eddies were excluded. The resultant WBC flow is illustrated within the red lines in Figure 6. Further notes on the chosen flow are as follows: at Port Shepstone (Figure 6b) there is evidence for an elongated anticyclonic feature at the eastern end of the section. It is not clear whether the circulation is closed (altimeter shows complex flow, Figure 3), but by including the northward and southward flow associated with it, its transport contribution should be more or less canceled. At East London (34°S) we exclude weak, deep flows within error bars, since western boundary current structure is not evident below about 2000 m (Figure 6c). At Port Elizabeth (36°S, Figure 6d), the northward and southward flows associated with the shear edge eddy are included, in order to cancel out its contribution. This is more accurate than trying to pinpoint the division of the southward flow in the Agulhas from that in the eddy. However, the deep northward flow associated with the undercurrent is excluded. Tests of other reasonable definitions for the boundaries of the Agulhas Current transport integration suggested that the sensitivity of the total transport to the choice of boundary definition is of order 5 Sv.

[40] The computed net mass transports from the above defined Agulhas Current are summarized in the schematic of Figure 5. At the northern most section the transport is 52 ± 4 Sv, increasing nonlinearly to 106 ± 8 Sv at the southern most section. The largest differences between section (net) transports and the Agulhas Current transport

as we have defined it, are at Richards Bay (30°S) and East London (34°S), notably where offshore cyclones interacted with the flow.

[41] The inflow/outflow pattern through the offshore sections, excluding the eddies contribution, is also shown in Figure 5. There remain significant entrainment/detrainment transports into/out of the Agulhas Current. Maximum entrainment was through the northernmost offshore section (PS-RB, between 32°S and 30°S), consistent with the large increase in Agulhas transport between these latitudes. The remaining two offshore sections (PE-EL and EL-PS), corresponded to an outflow (EL-PS) and inflow (PE-EL) into the Agulhas Current of similar size, contributing to a decrease in Agulhas transport between PS and EL, followed by a sharp increase between East London and Port Elizabeth.

4.4. Barotropic-Baroclinic Components of the Agulhas Current

[42] As noted above, the Agulhas Current transport increased from 52 ± 4 Sv at 30°S to 106 ± 8 Sv at 36°S, but this increase was not monotonic. One possibility is that fast moving barotropic variability was present and was aliased by our quasi-synoptic survey (one month duration). This could be the case at Port Shepstone, where the transport was high compared to *Bryden et al.*'s [2005] mean and a strong barotropic structure is evident in LADCP data. Another possibility is that inertial recirculations played a role. After removal of the baroclinic eddy fluxes, there remained large onshore/offshore flows of barotropic nature which could be attributed to inertial fluxes, particularly between East London and Port Elizabeth, where the Agulhas Current becomes detached from the continental slope. Here we investigate these mechanisms further.
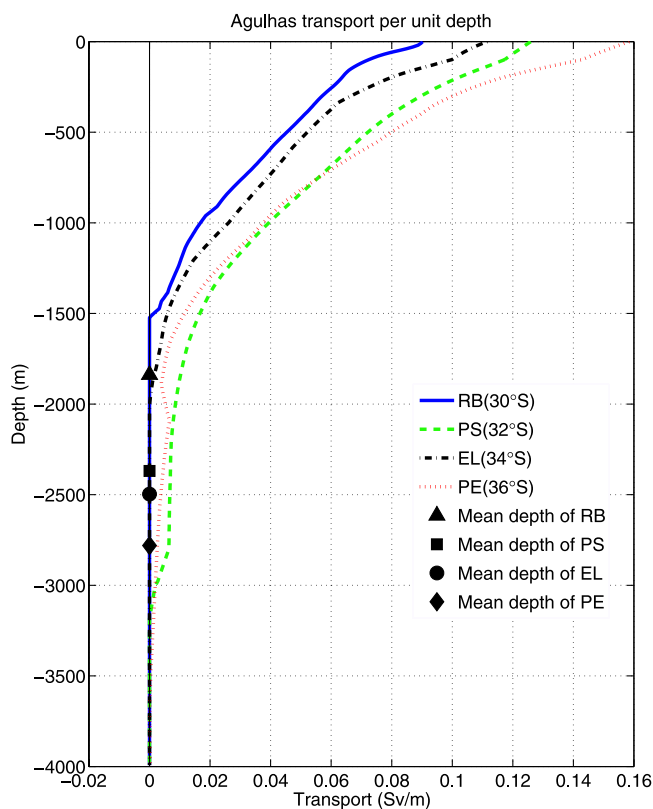
Figure 8. Vertical profiles of the Agulhas Current transport per unit depth (in Sv/m) for each cross section. The black symbols indicate the mean depth of each cross section.

[43] In an "equilibrium" state, the Sverdrup flow ought to be mainly an upper ocean flow [*Veronis and Stommel*, 1956], whereas inertial or eddy-driven recirculations tend to be barotropic [*Hogg*, 1992; *Johns et al.*, 1995]. However, fast time scale transport fluctuations are also primarily barotropic [*Stammer et al.*, 2001] but distinguishable from the latter because of their lack of systematic variation. Therefore, in an attempt to isolate wind-driven and local recirculating components of the Agulhas Current and determine whether the observed transport changes are consistent with dynamical expectations, the total transport of the Agulhas Current was decomposed into baroclinic and barotropic transports.

[44] The definitions used for "barotropic" and "baroclinic" components of the transport vary from author to author, and the choice of a particular definition seems to depend on the data set and the particular characteristics of the current in question. Therefore, the transport per unit depth for each cross section was first analyzed in order to understand how the transport structure changed between sections, to help us determine the definition that is most appropriate for the Agulhas Current. The transport per unit depth for the Agulhas Current proper (as defined above) at each section is displayed in Figure 8. Recall that these calculations include LNM information from LADCP. In all cross sections, the bulk of the transport and shear was located in the upper 1500 m of the water column. However, Richards Bay (at 30°S and the shallowest section) reached

zero transport around 1500 m, whereas at Port Shepstone (at 32°S) the transport reached zero at 3100 m. At East London (34°S) and Port Elizabeth (36°S) the transport became zero at 1900 m and 3500 m respectively. Therefore, at both Port Shepstone (32°S) and Port Elizabeth (36°S), the Agulhas Current reached into the deep layer, carrying some NADW southward. With the exception of Port Shepstone, a progressive deepening of the shear structure existed (Figure 8), considering the top of the shear structure as being the level where the curves became vertical. This deepening is in line with a southward increase in bottom depth.

[45] Classically, the term barotropic has meant depth invariant, while baroclinic has meant depth varying, although these definitions are not universal. For instance, *Hogg* [1992], in his study of the Gulf Stream mooring data between Cape Hatteras and the Grand Banks, defined the baroclinic contribution to the total transport as the integral of the transport per unit depth above an assumed LNM at 1000 m, while the barotropic component was the remaining transport. In our case, we need to define a different LNM since the observed shear in the Agulhas Current extends significantly below 1000 m (Figure 8). We therefore choose a reference level where the shear becomes zero at each section and set the baroclinic transport as the integrated transport to the surface relative to this level, and analogous to *Hogg* [1992], define the barotropic transport as the remainder. In other words, the baroclinic transport as defined here is the ocean transport that can clearly be identified with shear flow, while the barotropic transport is the top-to-bottom transport associated with the remaining barotropic flow beneath the shear layer.

[46] Analysis of the downstream evolution of the baroclinic and barotropic transports (Figure 9; corresponding values are given in Table 2) indicates barotropic transports not significantly different from zero, except at Port Shepstone (32°S), so that the baroclinic transport change closely reflects the total transport change. We acknowledge that a
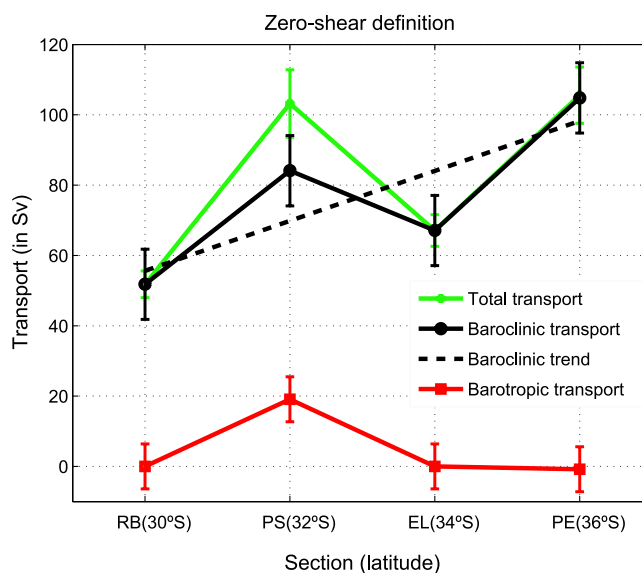

Figure 9. Total, barotropic and baroclinic transports (and associated trend) for the Agulhas Current (in Sv) at each cross section. Error bars given are standard errors.

Table 2. Downstream Change of the Agulhas Current Total Transport, Its Baroclinic and Barotropic Components Calculated Using the Zero-Shear Definition, and Associated Errors[a]

Transport (Sv)	RB (30°S)	PS (32°S)	EL (34°S)	PE (36°S)
Baroclinic	51.9 ± 10.0	84.1 ± 10.0	67.1 ± 10.0	104.8 ± 10.0
Barotropic	0 ± 6.4	19.1 ± 6.4	0 ± 6.4	−0.8 ± 6.4
Total	51.9 ± 3.8	103.2 ± 9.6	67.1 ± 4.5	105.6 ± 8.0
Sverdrup	44.6 ± 4.7	47.6 ± 3.4	57.7 ± 3.7	68.9 ± 5.1

[a]The errors for the baroclinic and barotropic components are calculated as the square root of the sum of the squares of the independent sources of error such as the sensitivity to the choice of Agulhas Current, LADCP error and temporal variability (for the baroclinic component only) and the value given is an upper limit. The Sverdrup transport is also shown along with its associated interannual variability (standard deviation). Units are in Sv.

different choice of barotropic/baroclinic could yield different results, but using two other definitions (*Hogg*'s [1992] and a LNM at 1500 m for all cross sections) the overall trends were similar, even though the transports in the individual sections differed. Furthermore, although the deep shears at Port Elizabeth are small, the velocity field at depth (from LADCP, Figure 6d) shows WBC structure, in contrast to the deep flow at Port Shepstone (Figure 6b).

[47] In keeping with *Hogg* [1992], we proceeded with the hypothesis that downstream variations in the baroclinic transport indicate baroclinic inflows or outflows for the current associated with the wind-driven Indian Ocean subgyre, while systematic changes in the barotropic transport are

associated with other processes such as depth-independent recirculations of a more local scale (e.g., inertial recirculations). Therefore, the lack of a systematic downstream increase in the barotropic transport suggested that the barotropic feature at Port Shepstone (32°S) likely arose from a barotropic wave that was unrelated to any larger-scale pattern.

[48] The fact that we did not find convincing evidence for an inertial recirculation of the Agulhas Current was surprising to us. Inertial recirculations are well recognized features of the Gulf Stream [*Hogg*, 1992; *Johns et al.*, 1995] where a barotropic component is fed from recirculations located to the north and south of the Gulf Stream path. Indeed, inertial recirculations are thought to be ubiquitous features of WBCs after their separation from the coast [*Feron et al.*, 1998]. Hence, we anticipate that additional data downstream of Port Elizabeth, the approximate location of the Agulhas breaking away from the continental slope, may reveal the existence of such a feature.

[49] As regards the baroclinic transports, we propose that the wind-driven downstream transport growth of the Agulhas Current approximated the best fit line shown in Figure 9. The mean trend is 4.1 ± 0.4 Sv/100 km, calculated by a least squares fit to the transport at each of the four sections. Error bars on the baroclinic and barotropic transports were calculated taking into consideration the sensitivity of the transport to the choice of the Agulhas Current boundary (±1 Sv), the formal transport errors given by the inverse model solution (±5 Sv), and the temporal variability
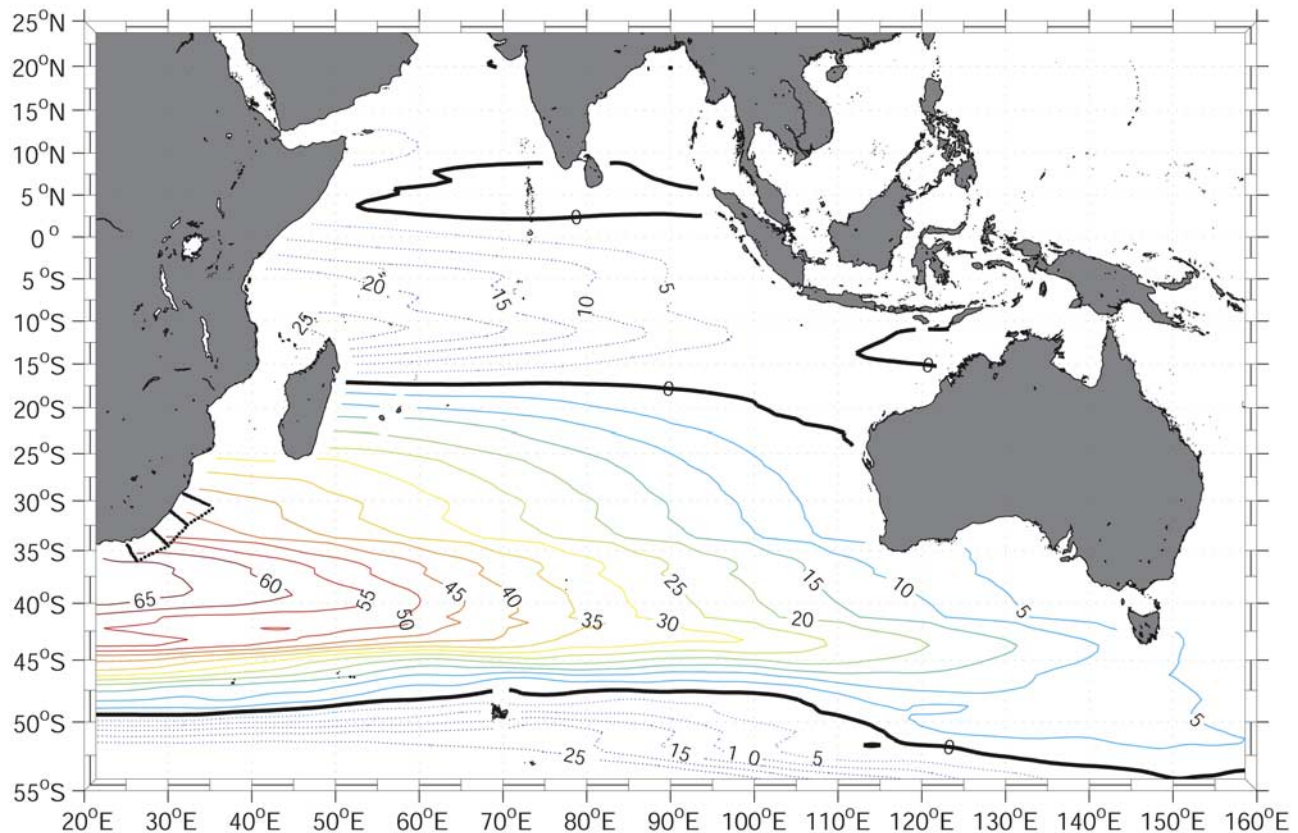

Figure 10. Indian Ocean Sverdrup transport (in Sv) calculated from August 1999 to January 2006 IFREMER monthly wind stress curl. The AUCE track is shown right next to the African continent.
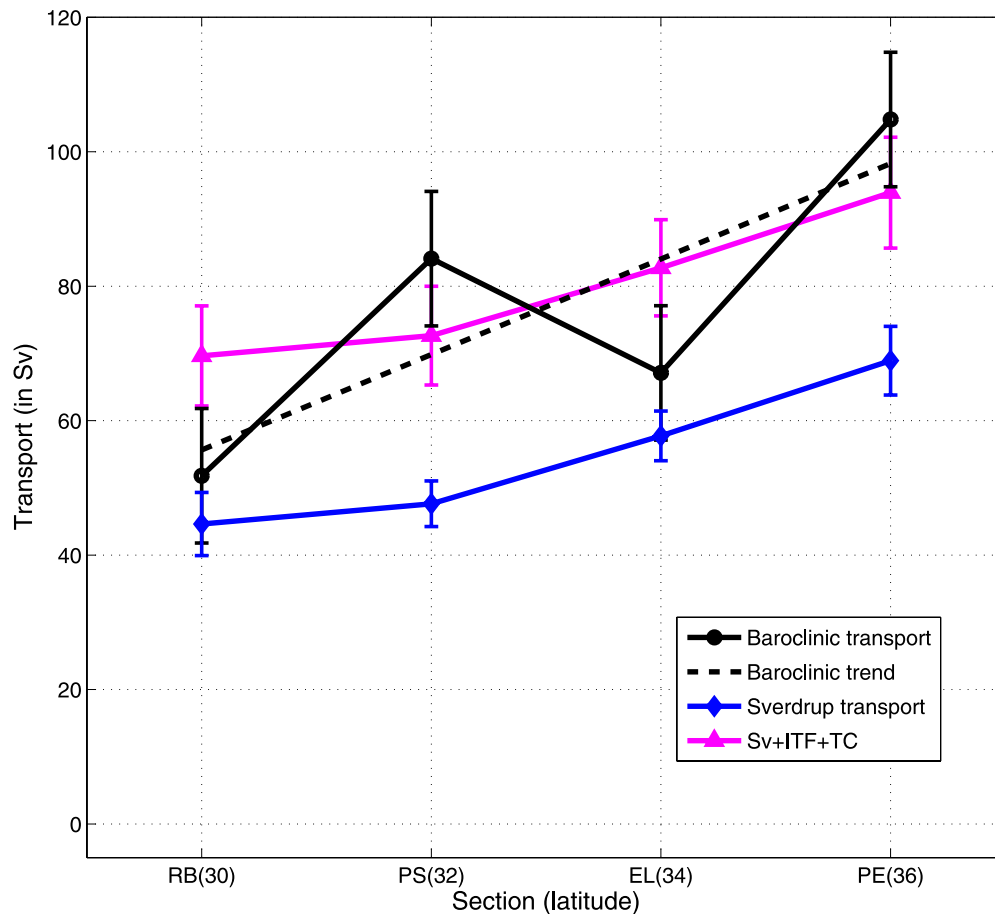
Figure 11. Downstream change of the baroclinic transport and corresponding trend versus the Sverdrup transport plus the Indonesian Throughflow transport (ITF) and the Indian Ocean overturning (TC). The vertical bars represent the standard errors, except in the Sverdrup transport where it represents the standard deviation of annual mean values.

which was only known in the baroclinic case. The temporal variability is an attempt to account for any differences between our quasi-synoptic data set and a time mean Agulhas Current. It is based on the standard deviation of the altimetric proxy time series of Agulhas Current transport as described previously, which is ±8.3 Sv.

[50] Is this gradient of downstream growth in baroclinic transport consistent with the expected wind-driven inflow from the South West Indian Ocean subgyre? In order to address this question, the theoretical meridional transport associated with the wind stress curl, i.e., the Sverdrup transport, was calculated as a function of latitude. The Sverdrup circulation was obtained by integrating the climatological IFREMER wind stress curl fields from the eastern boundary (landmasses on the eastern side including New Zealand) to the African coast. The time mean values of the Sverdrup circulation averaged over the 6 year period of the wind stress data are shown in Figure 10. The circulation is characterized by a counterclockwise gyre extending meridionally between [17–50]°S, and a clockwise gyre between [0°N–17°S]. The Sverdrup transport at each Agulhas Current cross section's latitude increased from 44.6 Sv at the latitude of Richards Bay (30°S) to 68.9 Sv at Port Elizabeth (36°S) (see Figure 10 and Table 2). In order to have a measure of the size of the Sverdrup transport interannual

variability, the standard deviation of the yearly averages from 2000 to 2006 at the latitude of each cross section was calculated (Table 2). The values ranged from 3.7 Sv at East London (34°S) to 5.1 Sv at Port Elizabeth (36°S).

[51] Figure 11 shows the baroclinic transport and trend (as shown in Figure 9) together with the Sverdrup transport for comparison. Clearly, the baroclinic transport at each cross section of the Agulhas Current was significantly larger than the associated Sverdrup transport. However, the rate of downstream increase of the observed baroclinic transport (trend) resembles closely that of the Sverdrup transport.

[52] Finding that the baroclinic Agulhas Current transport is not entirely accounted for by the interior Sverdrup flow is qualitatively consistent with the conclusions of *Bryden et al.* [2005]. This discrepancy can be explained by considering the presence of two other flows: the Indonesian Throughflow (ITF) and the Indian Ocean (IO) overturning, which must eventually exit the Indian Ocean within the Agulhas Current, in order to close the Indian Ocean mass balance.

[53] The ITF, which is the only low-latitude connection between the world's oceans, is a system of currents carrying fresh and warm water through the Indonesian Seas, from the Pacific to the Indian Ocean [*Gordon and Fine*, 1996]. It crosses the Indian Ocean in the westward flow of the South Equatorial Current (SEC) [*Talley and Sprintall*, 2005]

where it is slowly diluted. *Song et al.* [2004] investigated the ITF pathways in the Indian Ocean and concluded that ultimately, all the ITF water exits the Indian Ocean via the Agulhas Current. Even though the ITF undergoes significant interannual variability [*Gordon and Fine*, 1996], following the signals of ENSO [*Murtugudde et al.*, 1998] and Indian Ocean dynamics [*Yamagata et al.*, 1996], it is accepted that the *Ganachaud et al.* [2000] estimate of 15 ± 5 Sv (error value represents a one standard deviation level) is a good approximation of the ITF annual mean volume transport. The later estimate is roughly consistent with *Gordon et al.* [1999] ITF transport of about 10 Sv and *Lumpkin and Speer* [2007] of 13.3 ± 1.8 Sv.

[54] We also argue that the Agulhas Current carries a branch of the IO overturning circulation. In the decade mean global box inverse model of *Lumpkin and Speer* [2007], a deep northward flow across 32°S of around 12 ± 3 Sv is transformed to lighter layers (upper circumpolar deep water to intermediate water densities) and returns southward mostly west of 33°E within the Agulhas Current. This circulation pattern agrees with the one obtained by *Robbins and Toole* [1997] and *Ganachaud et al.* [2000], but differs from a recent model study by *Drijfhout and Garabato* [2008] who obtained a weak overturning of 5.6 Sv, and concluded that only 0.5 Sv of the IO overturning leaves the Indian Ocean via the Agulhas Current. We use *Ganachaud et al.* [2000] estimate of 10.6 ± 4 Sv, as it has an error bar that can reasonably accommodate interannual variability and is not significantly different than most of these other estimates.

[55] Comparison of the combined Sverdrup, ITF and IO overturning transports with the observed baroclinic transports (Figure 11; and assuming the ocean was close to baroclinic equilibrium, i.e., a forcing period much longer than the baroclinic adjustment time), showed that within the error bars, the magnitude of the observed baroclinic transport of the Agulhas Current was consistent with the Sverdrup + ITF + IO overturning transports at all AUCE latitudes. Note that a similar conclusion would be reached in all sections if we had used the total transport instead of the baroclinic transport.

5. Conclusions

[56] This study provided a detailed description of the Agulhas Current structure and its downstream variations during the Agulhas Undercurrent Experiment, that took place in February and March 2003. During AUCE, the (section-wide) Agulhas transport at the historic 32°S section was 100 ± 9 Sv, considerably higher than the yearlong current meter mean of 69.7 ± 21.5 Sv from *Bryden et al.* [2005]. Although high, this transport lies within the peak-to-peak variability of Bryden's transport time series.

[57] Several different types of eddies were observed during AUCE. Predominantly, cyclonic eddies were identified. Anticyclones were present offshore of the Agulhas Current, but were highly anisotropic and more intrinsic to the edge structure of the jet. A shear–edge cyclone was found at 36°S, between the current core and the continental slope. It reached down to the bottom of the intermediate layer (∼2000 m), with a radius ∼40 km and carried 19 ± 1 Sv of water. The remaining two cyclonic eddies were

sampled offshore of the current core, where the Richards Bay (30°S) and East London (34°S) cross sections intersect the offshore sections. These features were of mesoscale dimensions (∼100 km radius), reached into the intermediate layer and were both locally formed since their water properties did not differ from their environment. The RB cyclonic eddy carried 21 ± 3 Sv of water while the EL cyclonic eddy had a transport of 14 ± 4 Sv. These offshore eddies accounted for 30% of the total transport through the offshore sections.

[58] Within the inverse model framework, two experiments were set up, named the geostrophic and LADCP experiments. The first had initial conditions based on traditional water mass analysis, the second based on direct velocity information from LADCP. Both inverse model runs yielded similar results from the surface to the thermocline layers, but they differed significantly in the intermediate and deep layers. Furthermore, much stronger inflow/outflow through the offshore sections was found in the LADCP experiment compared to the geostrophic one. An Agulhas undercurrent was reproduced in the LADCP experiment, but did not exist in the geostrophic experiment (owing to the a priori LNM). Since the LADCP experiment gave a more realistic flow field, we used its results to give scientific insight into the fluxes of the Agulhas Current system.

[59] A consistent three dimensional picture of the Agulhas Current system between 30°S and 36°S was derived from our LADCP inverse solution, albeit based on a quasi-synoptic survey. During AUCE, the section integrated transports did not monotonically increase from the northernmost section to the southernmost one, as would be expected in the time-averaged case. Instead, a large increase occurred between Richards Bay (30°S) and Port Shepstone (32°S) where the section transport peaked at 100 ± 9 Sv, followed by a transport decrease at East London (34°S) and another increase at Port Elizabeth (36°S). These downstream changes in transport were a consequence of the large transports through the offshore sections. A similar picture emerged when the Agulhas transport was isolated from each of the cross-stream sections, excluding any observed eddies or counterflows.

[60] In an effort to understand the downstream transport variation, we first carefully defined the limits of the Agulhas Current and then separated the transport into baroclinic and barotropic components. Under these definitions, most of the transport change for the Agulhas Current was concentrated in the baroclinic component, reaching a maximum at the southern most section of 105 ± 10 Sv. The best fit trend in downstream baroclinic transport growth of the Agulhas Current could be explained, within error bars, by the Sverdrup transport associated with the wind pattern over the southern Indian Ocean. In order to match the total magnitude of the observed transports, the Indonesian Throughflow and the Indian Ocean Overturning needed to be taken into consideration.

[61] Only at Port Shepstone (32°S), where the Agulhas Current reached the seabed, was the barotropic component of the flow significant (20 ± 6 Sv). Hence, there is no evidence for an inertial recirculation in the AUCE region (a recognized feature at the separations of all major western boundary currents) which would manifest as a systematic growth of its barotropic component. Furthermore, the trans-

port budget can be balanced without invoking such a feature. In the case of the Gulf Stream, inertial recirculations grow once the current has detached from the continental slope at Cape Hatteras. In the Agulhas Current, only at the southernmost section has the current detached from the slope. Therefore future measurements farther south of this separation may provide evidence for an Agulhas Current inertial recirculation.

[62] In their 2005 paper, *Bryden et al.* [2005] found that the Agulhas transport was 50% higher than the Sverdrup transport would predict. They concluded that there was no consistent relationship between the measured size of the world's WBCs and their predicted Sverdrup transport. Here, we have shown that the Agulhas Current downstream transport increase is consistent with the downstream increase in Sverdrup transport (within error bars), and that its higher magnitude can be accounted for by including the Indian Ocean Overturning and the Indonesian Throughflow.

References

Arhan, M., H. Mercier, and Y.-H. Park (2003), On the deep water circulation of the eastern south Atlantic Ocean, *Deep Sea Res., Part I, 50*, 889–916, doi:10.1016/S0967-0637(03)00072-4.

Beal, L. M., and H. L. Bryden (1997), Observations of an Agulhas Undercurrent, *Deep Sea Res., Part I, 44*, 1715–1724, doi:10.1016/S0967-0637(97)00033-2.

Beal, L. M., and H. L. Bryden (1999), The velocity and vorticity structure of the Agulhas Current at 32°S, *J. Geophys. Res., 104*(C3), 5151–5176, doi:10.1029/1998JC900056.

Boebel, O., J. Lutjeharms, C. Schmid, W. Zenk, T. Rossby, and C. Barron (2003a), The Cape Cauldron: A regime of turbulent inter-ocean exchange, *Deep Sea Res., Part II, 50*, 57–86, doi:10.1016/S0967-0645(02)00379-X.

Boebel, O., T. Rossby, J. Lutjeharms, W. Zenk, and C. Barron (2003b), Path and variability of the Agulhas Return Current, *Deep Sea Res., Part II, 50*, 35–56, doi:10.1016/S0967-0645(02)00377-6.

Bryden, H. L., and L. M. Beal (2001), Role of the Agulhas Current in Indian Ocean circulation and associated heat and freshwater fluxes, *Deep Sea Res., Part I, 48*, 1821–1845, doi:10.1016/S0967-0637(00)00111-4.

Bryden, H. L., L. M. Beal, and L. M. Duncan (2005), Structure and transport of the Agulhas Current and its temporal variability, *J. Oceanogr., 61*, 479–492, doi:10.1007/s10872-005-0057-8.

Cessi, P., G. Ierley, and W. Young (1987), A model of the inertial recirculation driven by potential vorticity anomalies, *J. Phys. Oceanogr., 17*, 1640–1652, doi:10.1175/1520-0485(1987)017<1640:AMOTIR>2.0.CO;2.

Chereskin, T. K., and D. Roemmich (1991), A comparison of measured and wind-derived Ekman transport at 11°N in the Atlantic Ocean, *J. Phys. Oceanogr., 21*, 869–878, doi:10.1175/1520-0485(1991)021<0869:ACOMAW>2.0.CO;2.

De Ruijter, W. P. M., A. Biastoch, S. S. Drijfhout, J. R. E. Lutjeharms, R. P. Matano, T. Pichevin, P. J. van Leeuwen, and W. Weijer (1999a), Indian-Atlantic interocean exchange: Dynamics, estimation and impact, *J. Geophys. Res., 104*(C9), 20,885–20,910, doi:10.1029/1998JC900099.

De Ruijter, W. P. M., P. J. van Leeuwen, and J. R. E. Lutjeharms (1999b), Generation and evolution of natal pulses: Solitary meanders in the Agulhas Current, *J. Phys. Oceanogr., 29*(12), 3043–3055, doi:10.1175/1520-0485(1999)029<3043:GAEONP>2.0.CO;2.

Donohue, K. A., E. Firing, and L. Beal (2000), Comparison of three velocity sections of the Agulhas Current and Agulhas Undercurrent, *J. Geophys. Res., 105*(C12), 28,585–28,593.

Drijfhout, S. S., and A. C. N. Garabato (2008), The zonal dimension of the Indian Ocean Meridional Overturning Circulation, *J. Phys. Oceanogr., 38*(2), 359–379, doi:10.1175/2007JPO3640.1.

Duncan, C. P. (1968), An eddy in the Subtropical Convergence southwest of South Africa, *J. Geophys. Res., 73*(2), 531–534, doi:10.1029/JB073i002p00531.

Feron, R. C. V., W. P. M. de Ruijter, and P. J. van Leeuwen (1998), A new method to determine the mean sea surface dynamic topography from satellite altimeter observations, *J. Geophys. Res., 103*(C1), 1343–1362, doi:10.1029/97JC00389.

Firing, E. F. (1998), Lowered ADCP development and use in WOCE, *Int. WOCE Newsl., 30*, 10–14.

Fischer, J., and M. Visbeck (1993), Deep velocity profiling with self-contained ADCPs, *J. Atmos. Oceanic Technol., 10*, 764–773, doi:10.1175/1520-0426(1993)010<0764:DVPWSC>2.0.CO;2.

Ganachaud, A. S. (1999), Large scale oceanic circulation and fluxes of freshwater, heat, nutrients and oxygen, Ph.D. thesis, 249 pp., MIT-WHOI Joint Program, Woods Hole, Mass.

Ganachaud, A. S. (2003), Error budget of inverse box models: The North Atlantic, *J. Atmos. Oceanic Technol., 20*, 1641–1655, doi:10.1175/1520-0426(2003)020<1641:EBOIBM>2.0.CO;2.

Ganachaud, A. S., C. Wunsch, J. Marotzke, and J. Toole (2000), Meridional overturning and large-scale circulation of the Indian Ocean, *J. Geophys. Res., 105*(C11), 26,117–26,134, doi:10.1029/2000JC900122.

Gordon, A. L. (1985), Indian-Atlantic transfer of thermocline water at the Agulhas Retroflection, *Science, 227*, 1030–1033, doi:10.1126/science.227.4690.1030.

Gordon, A. L., and R. A. Fine (1996), Pathways of water between the Pacific and Indian oceans in the Indonesian seas, *Nature, 379*(6561), 146–149, doi:10.1038/379146a0.

Gordon, A. L., R. D. Susanto, and A. Ffield (1999), Throughflow within the Makassar Strait, *Geophys. Res. Lett., 26*, 3325–3328.

Gründlingh, M. L. (1980), On the volume transport of the Agulhas Current, *Deep Sea Res., Part A, 27*, 557–563, doi:10.1016/0198-0149(80)90040-0.

Hellerman, S., and M. Rosenstein (1983), Normal monthly wind stress over the world ocean with error estimates, *J. Phys. Oceanogr., 13*, 1093–1104, doi:10.1175/1520-0485(1983)013<1093:NMWSOT>2.0.CO;2.

Hogg, N. G. (1992), On the transport of the Gulf Stream between Cape Hatteras and the Grand Banks, *Deep Sea Res., Part A, 39*, 1231–1246, doi:10.1016/0198-0149(92)90066-3.

Hogg, N. G., and W. E. Johns (1995), Western boundary currents, *Rev. Geophys., 33*(S1), 1311–1334, doi:10.1029/95RG00491.

Johns, W. E., T. J. Shay, J. M. Bane, and D. R. Watts (1995), Gulf Stream structure, transport, and recirculation near 68°W, *J. Geophys. Res., 100*(C1), 817–838, doi:10.1029/94JC02497.

Le Traon, P.-Y., and F. Ogor (1998), ERS-1/2 orbit improvement using TOPEX/POSEIDON: The 2 cm challenge, *J. Geophys. Res., 103*, 8045–8057, doi:10.1029/97JC01917.

Levitus, S., and T. Boyer (1994), *World Ocean Atlas 1994*, vol. 4, *Temperature, NOAA Atlas NESDIS*, vol. 4, 117 pp., NOAA, Silver Spring, Md.

Lumpkin, R., and K. Speer (2003), Large-scale vertical and horizontal circulation in the North Atlantic Ocean, *J. Phys. Oceanogr., 33*, 1902–1920, doi:10.1175/1520-0485(2003)033<1902:LVAHCI>2.0.CO;2.

Lumpkin, R., and K. Speer (2007), Global ocean meridional overturning, *J. Phys. Oceanogr., 37*(10), 2550–2562, doi:10.1175/JPO3130.1.

Lutjeharms, J. R. E. (2006), *The Agulhas Current*, 329 pp., Springer, Berlin.

Lutjeharms, J. R. E., and H. R. Roberts (1988), The Natal pulse: An extreme transient on the Agulhas Current, *J. Geophys. Res., 93*(C1), 631–645.

Lutjeharms, J. R. E., O. Boebel, and H. T. Rossby (2003), Agulhas cyclones, *Deep Sea Res., Part II, 50*, 13–34, doi:10.1016/S0967-0645(02)00378-8.

Munk, W. H. (1950), On the wind-driven ocean circulation, *J. Meteorol., 7*(2), 79–93.

Murtugudde, R., A. J. Busalacchi, and J. Beauchamp (1998), Seasonal to interannual effects of the Indonesian Throughflow on the tropical Indo-Pacific Basin, *J. Geophys. Res., 103*, 21,425–21,441.

Pearce, A. F. (1977), Some features of the upper 500 m of the Agulhas Current, *J. Mar. Res., 35*, 731–753.

Pearce, A. F., and M. L. Gründlingh (1982), Is there a seasonal variation in the Agulhas Current?, *J. Mar. Res., 40*(1), 177–184.

Rio, M.-H., and F. Hernandez (2004), A mean dynamic topography computed over the world ocean from altimetry, in situ measurements, and a geoid model, *J. Geophys. Res., 109*, C12032, doi:10.1029/2003JC002226.

Robbins, P. E., and J. M. Toole (1997), The dissolved silica budget as a constraint on the Meridional Overturning Circulation of the Indian Ocean, *Deep Sea Res., Part I, 44*(5), 879–906, doi:10.1016/S0967-0637(96)00126-4.

Schouten, M. W., W. P. M. de Ruijter, and P. J. van Leeuwen (2002), Upstream control of Agulhas ring shedding, *J. Geophys. Res.*, *107*(C8), 3109, doi:10.1029/2001JC000804.

Sloyan, B. M., and S. R. Rintoul (2000), Estimates of area-averaged dia-pycnal fluxes from basin-scale budgets, *J. Phys. Oceanogr.*, *30*, 2320–2341, doi:10.1175/1520-0485(2000)030<2320:EOAADF>2.0.CO;2.

Sloyan, B. M., and S. R. Rintoul (2001), The Southern Ocean limb of the global deep overturning circulation, *J. Phys. Oceanogr.*, *31*, 143–173, doi:10.1175/1520-0485(2001)031<0143:TSOLOT>2.0.CO;2.

Song, Q., A. L. Gordon, and M. Visbeck (2004), Spreading of the Indone-sian Throughflow in the Indian Ocean, *J. Phys. Oceanogr.*, *34*, 772–792, doi:10.1175/1520-0485(2004)034<0772:SOTITI>2.0.CO;2.

Stammer, D., C. Böning, and C. Dieterich (2001), The role of variable wind forcing in generating eddy energy in the North Atlantic, *Prog. Oceanogr.*, *48*, 289–311.

Talley, L. D., and J. Sprintall (2005), Deep expression of the Indonesian Throughflow: Indonesian Intermediate Water in the South Equatorial Current, *J. Geophys. Res.*, *110*, C10009, doi:10.1029/2004JC002826.

Toole, J. M., and B. A. Warren (1993), A hydrographic section across the subtropical south Indian Ocean, *Deep Sea Res., Part I*, *40*, 1973–2019, doi:10.1016/0967-0637(93)90042-2.

Van Aken, H. M., H. Ridderinkhof, and W. P. M. De Ruijter (2004), North Atlantic deep water in the south-western Indian Ocean, *Deep Sea Res., Part I*, *51*, 755–776, doi:10.1016/j.dsr.2004.01.008.

van Leeuwen, P. J., W. P. M. De Ruijter, and J. R. E. Lutjeharms (2000), Natal pulses and the formation of Agulhas rings, *J. Geophys. Res.*, *105*(C3), 6425–6436, doi:10.1029/1999JC900196.

van Veldhoven, A. (2005), Observations of the evolution of Agulhas rings, Ph.D. dissertation, 159 pp., Univ. Utrecht, Utrecht, Netherlands.

Veronis, G., and H. Stommel (1956), The action of variable wind stresses on a stratified ocean, *J. Mar. Res.*, *15*, 43–75.

Visbeck, M. (2002), Deep velocity profiling using lowered acoustic Dop-pler current profilers: Bottom track and inverse solutions, *J. Atmos. Ocea-nic Technol.*, *19*, 794–807, doi:10.1175/1520-0426(2002)019<0794:DVPULA>2.0.CO;2.

Webb, D. J. (1999), An analytic model of the Agulhas Current as a western boundary current with linearly varying viscosity, *J. Phys. Oceanogr.*, *29*, 1517–1527, doi:10.1175/1520-0485(1999)029<1517:AAMOTA>2.0.CO;2.

Wunsch, C. (1996), *The Ocean Circulation Inverse Problem*, 442 pp., Cam-bridge Univ. Press, Cambridge, U. K.

Yamagata, T., K. Mizuno, and Y. Masumoto (1996), Seasonal variations in the equatorial Indian Ocean and their impacts on the Lambok Through-flow, *J. Geophys. Res.*, *101*, 12,465–12,473.

_____

L. M. Beal and W. E. Johns, MPO, RSMAS, University of Miami, Miami, FL 33149, USA.

T. G. D. Casal and R. Lumpkin, PhOD, AOML, NOAA, 4301 Rickenbacker Causeway, Miami, FL 33149, USA. (tania.casal@noaa.gov)